Supplementary Information to "Peak intervals of equatorial Pacific export production during the Middle Miocene Climate Transition"

Age Model

The age model employed in this study is modified from Tian et al. (2013) who created the original age model from the spliced composite section of Site U1337, with benthic $\delta^{18}O$ tuned to obliquity of the astronomical solution of Laskar et al. (2004). Ages for each sample were determined using linear extrapolation from the depth-age profile and shifted by -70 kyrs to better match the ages in Holbourn et al. (2014), based on the position of CM6 in the two records (Figure DR1). This modified age-depth relationship for Site U1337 was also applied to the XRF records from the same site (Shackford et al., 2014) to convert the weight percent data to accumulation rates.

BAR and CAR Analysis

Marine barite was separated from the samples following a sequential leaching procedure adapted from Paytan et al. (1996). Marine barite can dissolve in sediments if sulfate reducing conditions occur (McManus et al., 1998), however, analysis of interstitial waters show sulfate concentrations vary between 26 and 29 mM (Pälike et al., 2010), showing that the environment is not sulfate reducing. This procedure removes all sedimentary components except barite and a small amount of other resistant materials and was previously found to have a barite yield of ~95% (Eagle et al., 2003). The samples were screened for purity using scanning electron microscopy (SEM) after the sequential leaching procedure. It should be noted that the purity of the samples was verified prior to ashing, a modification to the original procedure adapted from Paytan et al. (1996). Impurities were identified on the SEM using the relative brightness of the grains in back-

scatter electron images (BSE) and confirmed with spot analysis using EDAX on the SEM. Five back-scatter images were taken of each sample (Figure DR2). Each image was analyzed for the percent of surface area that consisted of impurities using image analysis in MATLAB. Averaging the percent purity for each sample, the weight percent barite was calculated using this correction. The maximum correction corresponded to a barite weight percent of 86.21% in only one of the samples. The rest of the samples were over 92% barite, with an average of 98.5%.

The total inorganic carbon (TIC) for each sample was measured using a UIC, Inc. coulometer equipped with a CM5230 acidification module at the Bureau of Economic Geology in Austin, TX. The TIC was then converted to weight % $CaCO_3$ with the following equation:

$$\text{Weight \% } CaCO_3 = \frac{\text{TIC} \times 100}{12}$$

Mass accumulation rates (MAR) were determined using the following equation:

$$\text{MAR} = \text{LSR} \times \text{DBD}$$

Linear sedimentation rate (LSR) was calculated using the depth-age profile for Site U1337 modified from Tian et al. (2013) as outlined above. Dry bulk density (DBD) was estimated by linear interpolation between shipboard measurements (Pälike et al., 2010). Accumulation rates for barite (BAR) and $CaCO_3$ (CAR) were then calculated by multiplying the MAR by the weight percent of barite or $CaCO_3$, respectively. The CAR: BAR rain ratio is plotted in Figure DR3. The relationship between each record and MAR is shown in Figure DR4. Figure DR5 shows the relationship between each record, both as weight percent and accumulation rate. SiO_2AR has been interpolated from XRF data (Shackford et al., 2014) to find values equivalent in age to the discrete data (this study).

Calculation of Export Production

The determined BAR values were converted to export production rates (g C m^{-2} yr^{-1}) based on the present-day relationship between BAR and export production obtained from core top sediments from the EEP (Paytan et al., 1996; Eagle et al., 2003).

Spectral Analysis

Prior to analysis, each record was interpolated at 1-kyr steps, detrended, and normalized to ensure comparability. Power-spectral analysis was performed to uncover the average strength of orbital cycles in the U1337 records. Increased variability in the BAR signal after 13.8 Ma was observed, so the power-spectral analyses were done over two time periods, 14.1-13.75 Ma and 13.75-13.4 Ma, before and after this observed change in the record (Figure DR6). Cross-spectral analyses were also performed to evaluate coherent or noncoherent relationships between any two of the records (Figure DR7). These analyses were performed using MATLAB.

Carbon-Cycle Model

We investigated the potential global carbon cycle effects of the periods of elevated EEP export productivity indicated by BAR records using the Long-term Ocean-Sediment Carbon Reservoir (LOSCAR) model (Zeebe, 2012). LOSCAR is a numerically-efficient model that simulates the biogeochemical fluxes of several carbon-cycle and climate-relevant tracers between the atmosphere, oceans, and sediments on timescales of centuries to millions of years. We used the modern (pre-industrial) configuration of LOSCAR featuring modern ocean basin geometry and circulation, and an equilibrium atmospheric pCO_2 of 280 ppm, which is close to available pCO_2-proxy estimates for the Middle Miocene (Pagani et al., 1999; Foster et al., 2012).

In order to simulate the effects of increased export productivity, we manipulated LOSCAR's parameterization of the biological pump, which is described as the efficiency with which upwelled phosphate ($[PO_4^{3-}]$) is converted to sinking organic matter. The efficiency term (F_{EPL}) is by default set to 0.8 (tuned parameter from Zeebe [2012]), meaning that 80% of phosphate that upwells into the surface Pacific reservoir is converted to sinking particulate matter, taking along with it a quantity of organic carbon (export productivity) determined by a Redfield ratio (C:P = 130:1). By increasing the efficiency term (F_{EPL}) we can thus increase nutrient utilization and generate an increase in export productivity, as indicated by BAR records. Because net uptake of phosphate in the surface ocean is equivalent to particle export flux from the mixed layer, this also increases production at the surface. However, as the BAR records likely represent only the EEP (which represents only about 18% of the Pacific Ocean by area and 22% of its productivity; Pennington et al., 2006) and LOSCAR represents the entire surface Pacific as a single reservoir, an accounting has to be made for how much an increase in EEP productivity would change the productivity of the Pacific as a whole (which is what can be manipulated in LOSCAR). If, for example, EEP productivity increased by a factor of 2 and the rest of the Pacific remained the same, this would result in a total Pacific export productivity ~1.22 times higher. This is what is simulated in Figure DR8: an increase in Pacific F_{EPL} of 22% (from 0.8 to 0.976), drawing down surface phosphate concentrations to near zero and increasing $d^{13}C$ by ~0.2‰.

REFERENCES

Badger, M.P.S., Lear, C.H., Pancost, R.D., Foster, G.L., Bailey, T.R., Leng, M.J., and Abels, H.A., 2013, CO_2 drawdown following the middle Miocene expansion of the Antarctic Ice Sheet: Paleoceanography, v. 28, p. 42–53, doi:10.1002/palo.20015.

Eagle, M., Paytan, A., Arrigo, K.R., van Dijken, G., and Murray, R.W., 2003, A comparison between excess barium and barite as indicators of carbon export: Paleoceanography, v. 18, 1021, doi:10.1029/ 2002PA000793.

Erhardt, A.M, Pälike, H., and Paytan, A., 2013, High-resolution record of export production in the eastern equatorial Pacific across the Eocene-Oligocene transition and relationships to global climatic records: Paleoceanography, v. 28, doi:10.1029/2012PA002347.

Foster, G.L., Lear, C.H., and Rae, J.W., 2012, The evolution of pCO_2, ice volume and climate during the middle Miocene: Earth and Planetary Science Letters, v. 341-344, p. 243-254, doi:10.1016/j.epsl.2012.06.007.

Griffith, E.M., Calhoun, M., Thomas, E., Averyt, K., Erhardt, A., Bralower, T., Lyle, M., Olivarez-Lyle, A., and Paytan, A., 2010, Export productivity and carbonate accumulation in the Pacific Basin at the transition from a greenhouse to icehouse climate (late Eocene to early Oligocene): Paleoceanography, v. 25, PA3212, doi:10.1029/2010PA001932.

Holbourn, A., Kuhnt, W., Lyle, M., Schneider, L., Romero, O., and Anderson, N., 2014, Middle Miocene climate cooling linked to intensification of eastern equatorial Pacific upwelling: Geology, v. 42, p. 19-22, doi:10.1130/G34890.1.

Laskar, J., Robutel, P., Joutel, F., Gastineau, M., Correia, A.C.M., and Levrard, B., (2004), A long term numerical solution for the insolation quantities of the Earth: Astronomy and Astrophysics, v. 428, p. 261–285.

Ma, Z., Gray, E., Thomas, E., Murphy, B., Zachos. J., and Paytan, A., 2014, Carbon sequestration during the Palaeocene-Eocene Thermal Maximum by an efficient biological pump: Nature Geoscience, v. 7, p. 382-388.

Ma, Z. Ravelo, A.C, Liu, Z., Zhou, L., Paytan, A., 2015, Export production fluctuations in the eastern equatorial Pacific during the Pliocene-Pleistocene: Reconstruction using barite accumulation rates: Paleoceanography, v. 30, doi:10.1002/2015PA002860.

McManus, J., et al., 1998, Geochemistry of barium in marine sediments: Implications for its use as a paleoproxy: Geochimica Cosmochimica Acta, v. 62, p. 3453-3473.

Pagani, M., Arthur, M.A., and Freeman, K.H., 1999, Miocene evolution of atmospheric carbon dioxide: Paleoceanography, v. 14, p. 273-292, doi:10.1029/1999PA900006.

Pälike, H., Lyle, M., Nishi, H., Raffi, I., Gamage, K., Klaus, A., and the Expedition 320/321 Scientists, 2010, Pacific equatorial age transect: Proceedings of the Integrated Ocean Drilling Program Expedition 320/321: Tokyo, Integrated Ocean Drilling Program Management International, Inc., http://publications.iodp.org/proceedings/320_321/32021toc.htm.

Paytan, A., Kastner, M., Chavez, F.P., 1996, Glacial to Interglacial fluctuations in productivity in the Equatorial Pacific as indicated by marine barite: Science, v. 274, p. 1355-1357, doi:10.1126/science.274.5291.1355.

Pennington, J.T., Mahoney, K., Kuwahara, V., Kolber, D., Calienes, R., and Chavez, F., 2006, Primary production in the eastern tropical Pacific: A review: Progress in Oceanography, v. 69, p. 285-317.

Shackford, J.K., Lyle, M., Wilkens, R., and Tian, J., 2014, Data report: raw and normalized elemental data along the Site U1335, U1336, and U1337 splices from X-ray fluorescence scanning. In Pälike, H., Lyle, M., Nishi, H., Raffi, I., Gamage, K., Klaus, A., and the Expedition 320/321 Scientists, Proc. IODP, 320/321: Tokyo, Integrated Ocean Drilling Program Management International, Inc., doi:10.2204/iodp.proc.320321.216.2014.

Tian, J., Yang, M., Lyle, M.W., Wilkens, R., and Shackford, J.K., 2013, Obliquity and long eccentricity pacing of the Middle Miocene climate transition: Geochemistry, Geophysics, Geosystems: v. 14, p.1740-1755, doi: 10.1002/ggge.20108.

Wilkens, R.H., Dickens, G.R., Tian, J., Backman, J., and the Expedition 320/321 Scientists, 2013, Data report: revised composite depth scales for Sites U1336, U1337, and U1338. In H. Pälike, M. Lyle, H. Nishi, I. Raffi, K. Gamage, A. Klaus, and the Expedition 320/321 Scientists, Proc. IODP, 320/ 321: Tokyo (Integrated Ocean Drilling Program Management International, Inc.). doi:10.2204/iodp.proc.320321.209.2013.

Zeebe, R., 2012, LOSCAR: Long-term ocean-atmosphere-sediment carbon cycle reservoir model v2. 0.4: Geoscientific Model Development, v. 5, p. 149-166, doi:10.5194/gmd-5-149-2012.

SUPPLEMENTARY FIGURES

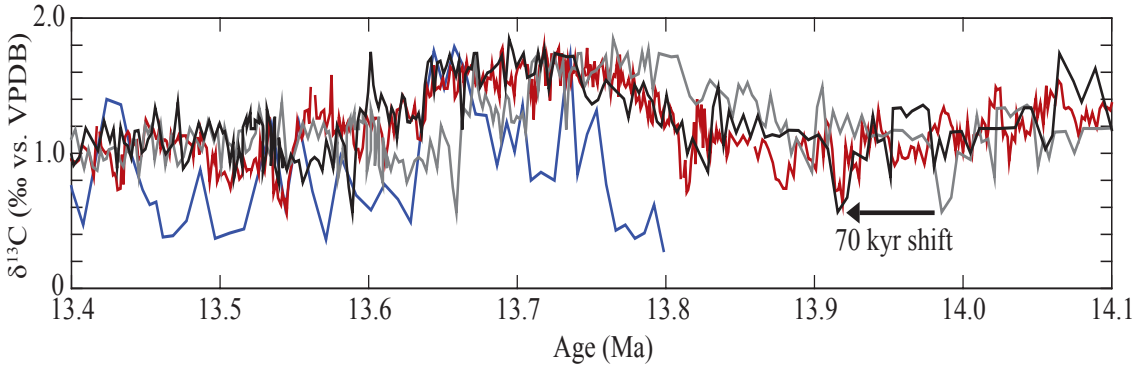

Figure DR1. Records of $\delta^{13}C$ showing the -70 kyr shift of the age model used in this study (Tian et al., 2013) to match the age model by Holbourn et al. (2014), based on the positions of the carbon maxima event 6 (CM6). Carbonate $\delta^{13}C$ from fine fraction of the Ras il-Pellegrin section (blue line; Badger et al., 2013); benthic foraminiferal $\delta^{13}C$ from IODP Site U1338 (red line; Holbourn et al., 2014); original benthic foraminiferal $\delta^{13}C$ from IODP Site U1337 (grey line; Tian et al., 2013); and benthic foraminiferal $\delta^{13}C$ from IODP Site U1337 (Tian et al., 2013) shifted -70 kyr (black line).

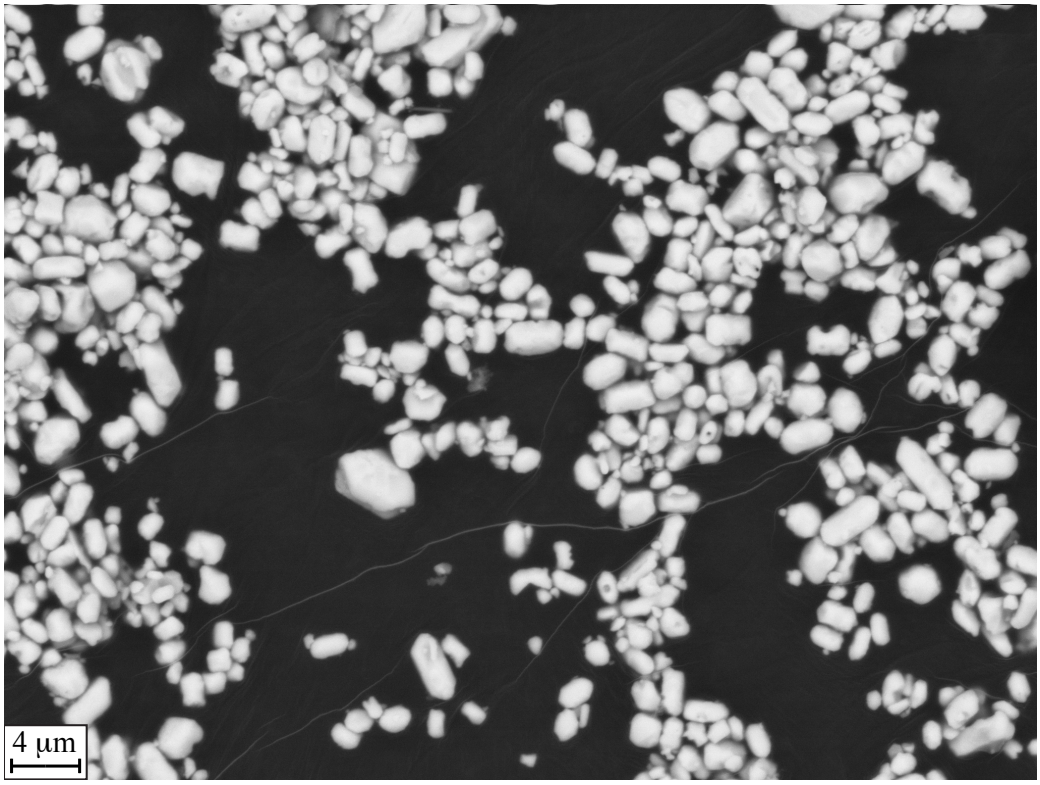

Figure DR2. Back-scatter electron (BSE) image of barite grains taken on the scanning electron microscope (SEM). Using our method of image analysis, this sample was found to have a barite purity of 99.8%.

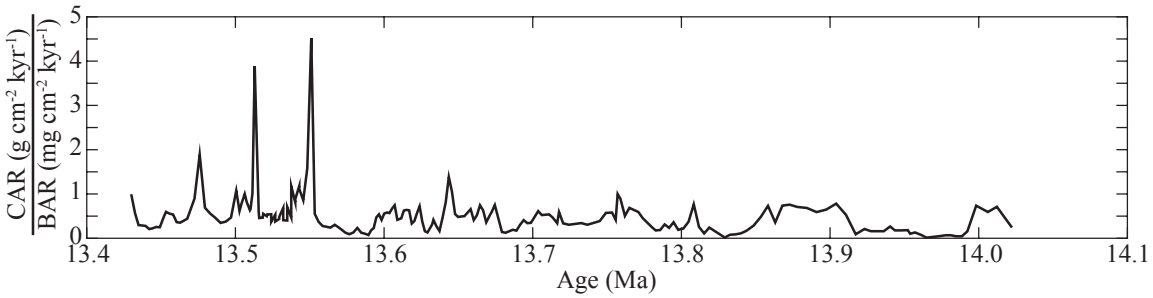

Figure DR3. Calculated rain ratio of calcium carbonate to organic carbon from U1337 (this study).

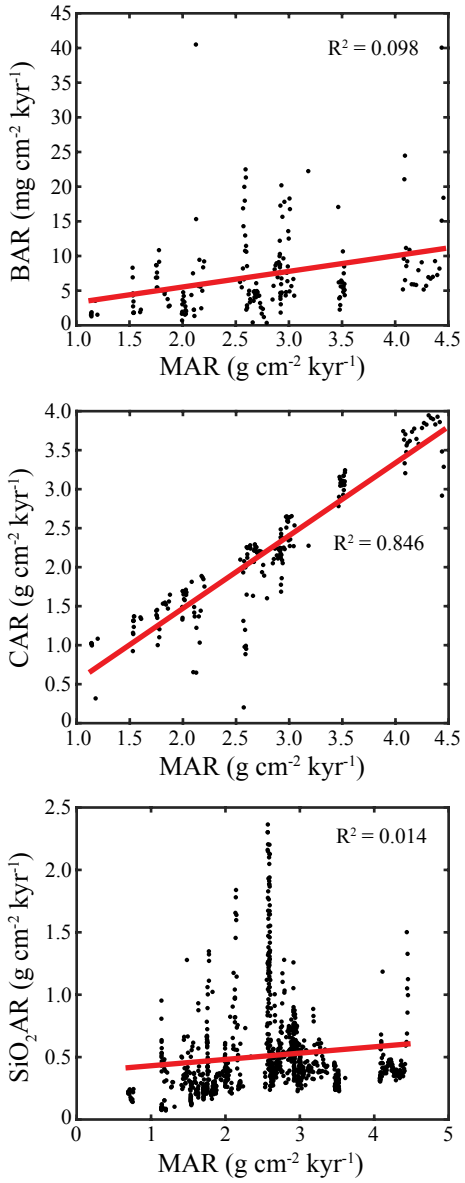

Figure DR4. Relationships between accumulation rate-based records and MAR. MAR calculated using a modified age model from Tian et al. (2013). BAR and CAR measured from discrete analysis (this study). SiO_2AR from XRF data (Shackford et al., 2014).

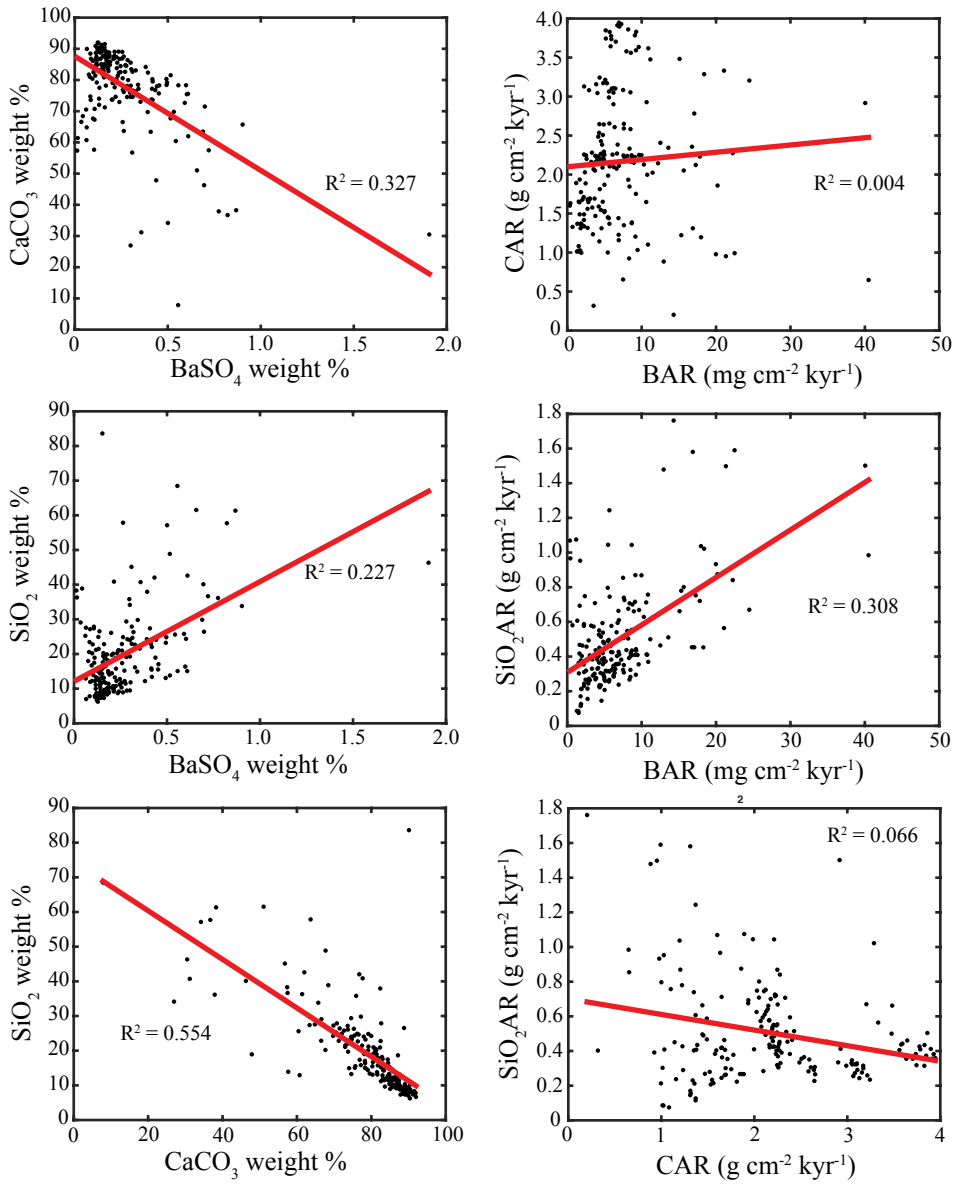

Figure DR5. Relationships between each record: Records shown as weight percent (left column). Records shown as accumulation rates (right column). Weight percent data are converted to accumulation rate using a modified age model from Tian et al. (2013). BAR, CAR and weight percent $BaSO_4$ and $CaCO_3$ measured from discrete analysis (this study). Weight percent SiO_2 and SiO_2AR from XRF data (Shackford et al., 2014).

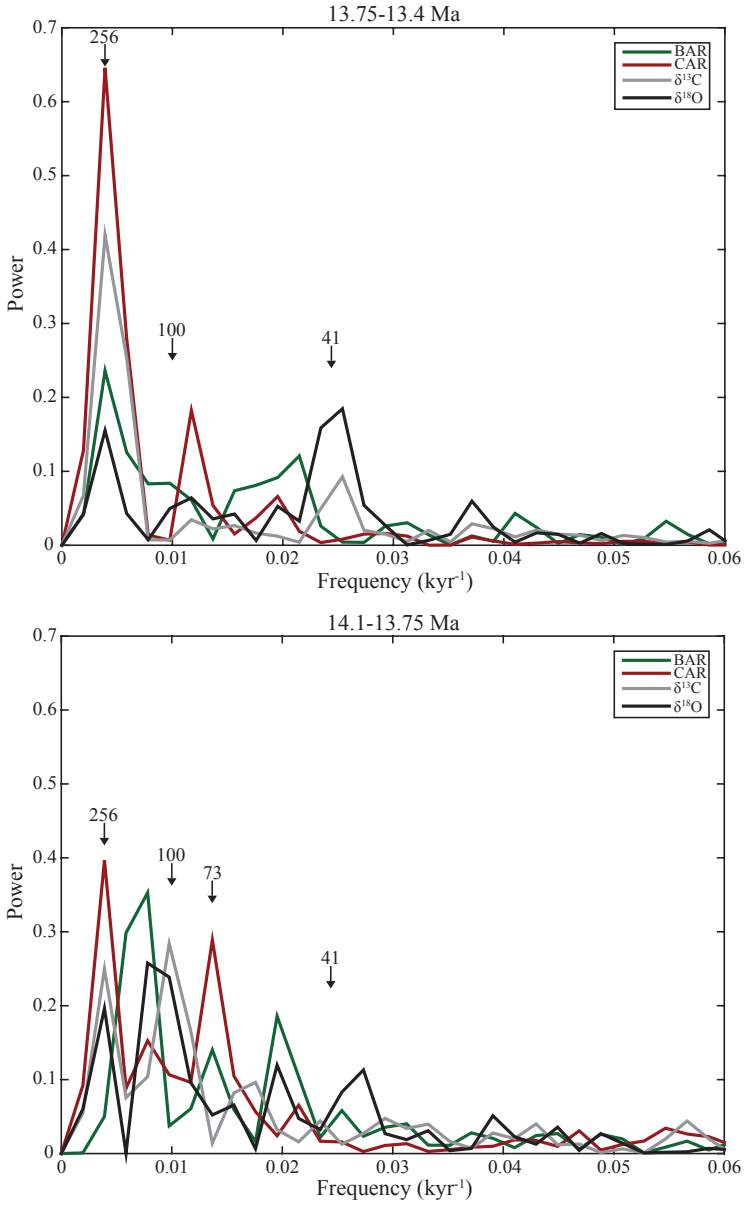

Figure DR6. Power-spectrum of barite accumulation rate (BAR) (green), $CaCO_3$ accumulation rate (CAR) (red), benthic foraminiferal $\delta^{13}C$ (grey; Tian et al., 2013), and benthic foraminiferal $\delta^{18}O$ (black; Tian et al., 2013). Note, there is a shift in power in both the $\delta^{13}C$ and $\delta^{18}O$ isotopic records over this time period from the 100-kyr cycle (eccentricity) to the 41-kyr cycle (obliquity), as previously found in Tian et al. (2013). The records of BAR and CAR do not show this trend.

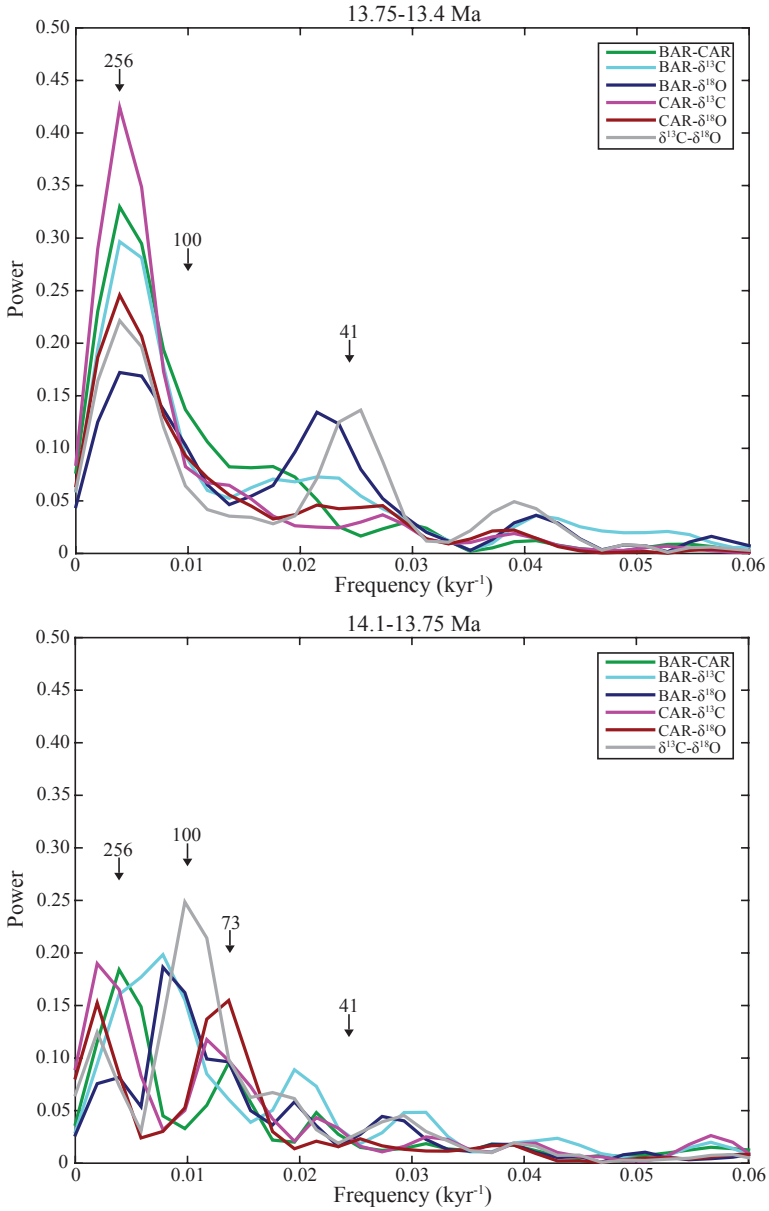

Figure DR7. Cross-spectral analysis of barite accumulation rate (BAR) and $CaCO_3$ accumulation rate (CAR) (green), BAR and benthic foraminiferal $\delta^{13}C$ (blue), BAR and benthic foraminiferal $\delta^{18}O$ (black), CAR and $\delta^{13}C$ (pink), CAR and $\delta^{18}O$ (red), and $\delta^{13}C$ and $\delta^{18}O$ (grey). $\delta^{13}C$ and $\delta^{18}O$ records from Tian et al. (2013). Again, note the shift of power in the $\delta^{13}C$ and $\delta^{18}O$ records from the 100-kyr to the 41-kyr cycle. Also, there is a higher magnitude of power between each of the records in the time period after 13.75 Ma.

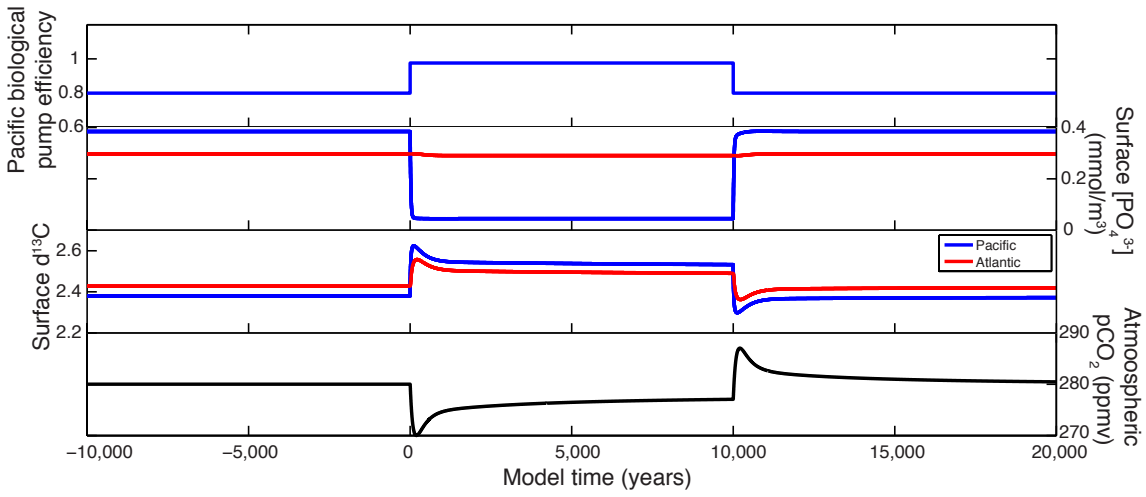

Figure DR8. Results for LOSCAR model run forced by an increase in Pacific F_{EPL} of 22% (from 0.8 to 0.976, top panel), which results a in draw-down of surface phosphate concentrations (second panel) to near zero within <1,000 years, and increase in surface Pacific $\delta^{13}C$ of ~0.2‰ (third panel), and a ~10ppm decrease in pCO_2, which occurs only within centuries, while there are still nutrients available .

Table DR1. Comparison of peak and average barite accumulation rates (BAR) in the eastern equatorial Pacific (EEP) during various geologic time periods.

Time Period	Peak BAR (mg cm^{-2} kyr^{-1})	Average BAR (mg cm^{-2} kyr^{-1})
Glacial/Interglacial cycles[a]	6	1.24
Pliocene-Pleistocene[b]	11	3.52
MMCT[c]	40	7.09
Eocene-Oligocene transition[d,e]	8	0.78
Paleocene-Eocene Thermal Maximum[f]	18	2.17

[a]Paytan et al. (1996); [b]Ma et al. (2015); [c]This study; [d]Griffith et al. (2010); [e]Erhardt et al. (2013); [f]Ma et al. (2014)

Table DR2. U1337 BAR and CAR (this study)

Site	Hole	Core	Type	Section	Top (cm)	Bottom (cm)	CCSF* (m)	Age** (Ma)	Shifted age (Ma)	MAR (g cm^{-2} kyr^{-1})	$CaCO_3$ weight %	CAR (g cm^{-2} kyr^{-1})	$BaSO_4$ weight %	BAR (mg cm^{-2} kyr^{-1})	Export C (gC m^{-2} yr^{-1})
U1337	D	31	X	3	78	80	305.47	13.50	13.43	2.92	60.73	1.77	0.06	1.84	28.27
U1337	D	31	X	3	86	88	305.55	13.50	13.43	2.92	74.03	2.16	0.13	3.81	46.62
U1337	D	31	X	3	94	96	305.63	13.50	13.43	2.92	76.86	2.24	0.26	7.55	81.35
U1337	D	31	X	3	102	104	305.71	13.51	13.44	2.92	76.16	2.22	0.26	7.69	82.63
U1337	D	31	X	3	110	112	305.79	13.51	13.44	2.92	79.98	2.33	0.29	8.37	89.00
U1337	D	31	X	3	118	120	305.87	13.51	13.44	2.92	73.02	2.13	0.35	10.29	106.87
U1337	D	31	X	3	126	128	305.95	13.51	13.44	2.91	77.19	2.25	0.34	9.97	103.90
U1337	D	31	X	3	134	136	306.03	13.52	13.45	2.91	75.92	2.21	0.30	8.66	91.72
U1337	D	31	X	3	142	144	306.11	13.52	13.45	2.92	74.58	2.18	0.30	8.76	92.63
U1337	D	31	X	4	2	4	306.21	13.52	13.45	2.92	81.61	2.38	0.16	4.68	54.69
U1337	D	31	X	4	6	8	306.25	13.52	13.45	2.92	85.11	2.49	0.14	4.16	49.86
U1337	D	31	X	4	14	16	306.33	13.53	13.46	2.92	57.66	1.69	0.10	3.03	39.38
U1337	D	31	X	4	22	24	306.41	13.53	13.46	2.92	83.03	2.43	0.15	4.53	53.28
U1337	D	31	X	4	30	32	306.49	13.53	13.46	2.93	73.75	2.16	0.20	5.94	66.36
U1337	D	31	X	4	38	40	306.57	13.53	13.46	2.93	81.35	2.38	0.23	6.77	74.12
U1337	D	31	X	4	54	56	306.73	13.54	13.47	2.93	71.24	2.09	0.16	4.74	55.21
U1337	D	31	X	4	66	68	306.85	13.54	13.47	1.99	74.75	1.49	0.08	1.67	26.68
U1337	D	31	X	4	74	76	306.93	13.55	13.48	1.99	66.59	1.33	0.04	0.70	17.73
U1337	D	31	X	4	82	84	307.01	13.55	13.48	2.00	67.66	1.35	0.10	1.96	29.39
U1337	D	31	X	4	90	92	307.09	13.55	13.48	2.00	84.80	1.69	0.15	3.03	39.37
U1337	D	31	X	4	98	100	307.17	13.56	13.49	2.00	84.60	1.69	0.18	3.67	45.30
U1337	D	31	X	4	106	108	307.25	13.56	13.49	2.01	82.33	1.65	0.24	4.76	55.48
U1337	D	31	X	4	114	116	307.33	13.56	13.49	2.01	79.13	1.59	0.21	4.23	50.49
U1337	D	31	X	4	122	124	307.41	13.57	13.50	2.02	78.21	1.58	0.17	3.37	42.51
U1337	D	31	X	4	130	132	307.49	13.57	13.50	2.02	81.75	1.65	0.08	1.54	25.48
U1337	C	15	X	2	95	97	307.54	13.57	13.50	2.03	83.00	1.68	0.14	2.74	36.65
U1337	D	31	X	4	138	140	307.57	13.57	13.50	2.03	84.39	1.71	0.11	2.20	31.63
U1337	C	15	X	2	103	105	307.62	13.58	13.51	2.03	81.01	1.64	0.08	1.64	26.47
U1337	D	31	X	4	146	148	307.65	13.58	13.51	2.03	82.49	1.68	0.10	2.04	30.15

Site	Hole	Core	Type	Section	Top (cm)	Bottom (cm)	CCSF* (m)	Age** (Ma)	Shifted age (Ma)	MAR (g cm^{-2} kyr^{-1})	$CaCO_3$ weight %	CAR (g cm^{-2} kyr^{-1})	$BaSO_4$ weight %	BAR (mg cm^{-2} kyr^{-1})	Export C (gC m^{-2} yr^{-1})
U1337	C	15	X	2	111	113	307.70	13.58	13.51	2.11	67.29	1.42	0.11	2.24	31.99
U1337	D	31	X	5	2	4	307.71	13.58	13.51	2.11	70.73	1.49	0.11	2.25	32.10
U1337	D	31	X	5	6	8	307.74	13.58	13.51	2.11	64.83	1.37	0.06	1.35	23.76
U1337	C	15	X	2	119	121	307.78	13.58	13.51	2.66	61.40	1.63	0.02	0.42	15.10
U1337	C	15	X	2	127	129	307.86	13.59	13.52	2.67	77.51	2.07	0.13	3.53	44.05
U1337	D	31	X	5	18	20	307.87	13.59	13.52	2.67	82.87	2.21	0.18	4.84	56.17
U1337	C	15	X	2	135	137	307.94	13.59	13.52	2.68	85.66	2.29	0.18	4.93	57.01
U1337	D	31	X	5	26	28	307.95	13.59	13.52	2.68	83.39	2.23	0.15	4.04	48.73
U1337	C	15	X	2	143	145	308.02	13.59	13.52	2.68	84.52	2.27	0.17	4.54	53.42
U1337	D	31	X	5	34	36	308.03	13.59	13.52	2.68	82.50	2.21	0.15	4.11	49.40
U1337	D	31	X	5	42	44	308.11	13.59	13.52	2.69	81.74	2.20	0.15	4.06	48.93
U1337	C	15	X	3	2	4	308.11	13.59	13.52	2.69	83.79	2.26	0.23	6.08	67.66
U1337	C	15	X	3	10	12	308.19	13.60	13.53	2.70	80.45	2.17	0.15	4.08	49.16
U1337	D	31	X	5	50	52	308.19	13.60	13.53	2.70	81.47	2.20	0.21	5.80	65.12
U1337	D	31	X	5	58	60	308.27	13.60	13.53	2.70	80.91	2.19	0.19	5.02	57.87
U1337	C	15	X	3	18	20	308.27	13.60	13.53	2.71	81.40	2.20	0.17	4.57	53.67
U1337	D	31	X	5	66	68	308.35	13.60	13.53	2.71	83.26	2.26	0.12	3.29	41.79
U1337	C	15	X	3	26	28	308.35	13.60	13.53	2.71	78.41	2.13	0.19	5.23	59.79
U1337	C	15	X	3	34	36	308.43	13.60	13.53	2.72	79.34	2.16	0.20	5.39	61.31
U1337	D	31	X	5	74	76	308.43	13.60	13.53	2.72	82.90	2.26	0.12	3.19	40.83
U1337	C	15	X	3	42	44	308.51	13.61	13.54	2.73	79.20	2.16	0.17	4.61	54.01
U1337	D	31	X	5	82	84	308.51	13.61	13.54	2.73	79.23	2.16	0.07	1.84	28.27
U1337	D	31	X	5	90	92	308.59	13.61	13.54	2.73	75.70	2.07	0.09	2.54	34.81
U1337	C	15	X	3	50	52	308.59	13.61	13.54	2.74	85.13	2.33	0.10	2.65	35.79
U1337	D	31	X	5	98	100	308.67	13.61	13.54	2.74	64.23	1.76	0.05	1.49	25.07
U1337	C	15	X	3	58	60	308.67	13.61	13.54	2.75	83.15	2.28	0.07	2.04	30.19
U1337	C	15	X	3	66	68	308.75	13.62	13.55	2.76	73.63	2.03	0.09	2.37	33.18
U1337	C	15	X	3	74	76	308.83	13.62	13.55	2.76	68.42	1.89	0.04	1.20	22.33
U1337	C	15	X	3	82	84	308.91	13.62	13.55	2.79	57.38	1.60	0.01	0.35	14.49
U1337	C	15	X	3	89	91	308.98	13.62	13.55	2.85	72.04	2.05	0.13	3.72	45.79

Site	Hole	Core	Type	Section	Top (cm)	Bottom (cm)	CCSF* (m)	Age** (Ma)	Shifted age (Ma)	MAR (g cm^{-2} kyr^{-1})	$CaCO_3$ weight %	CAR (g cm^{-2} kyr^{-1})	$BaSO_4$ weight %	BAR (mg cm^{-2} kyr^{-1})	Export C (gC m^{-2} yr^{-1})
U1337	C	15	X	3	97	99	309.06	13.63	13.56	2.86	73.71	2.10	0.20	5.69	64.12
U1337	C	15	X	3	105	107	309.14	13.63	13.56	2.87	78.08	2.24	0.28	8.07	86.19
U1337	C	15	X	3	113	115	309.22	13.63	13.56	2.87	78.18	2.25	0.30	8.65	91.59
U1337	C	15	X	3	121	123	309.30	13.63	13.56	2.88	74.58	2.15	0.31	8.95	94.38
U1337	C	15	X	3	130	132	309.39	13.64	13.57	2.89	72.96	2.11	0.24	6.94	75.70
U1337	C	15	X	3	138	140	309.47	13.64	13.57	2.90	76.58	2.22	0.31	9.11	95.88
U1337	C	15	X	3	146	148	309.55	13.64	13.57	2.91	73.60	2.14	0.42	12.20	124.57
U1337	C	15	X	4	2	4	309.61	13.64	13.57	2.92	72.67	2.12	0.59	17.27	171.68
U1337	C	15	X	4	10	12	309.69	13.65	13.58	2.93	63.46	1.86	0.69	20.19	198.89
U1337	C	15	X	4	18	20	309.77	13.65	13.58	2.94	69.82	2.05	0.53	15.65	156.68
U1337	C	15	X	4	26	28	309.85	13.65	13.58	2.95	76.36	2.25	0.33	9.65	100.92
U1337	C	15	X	4	34	36	309.93	13.65	13.58	2.96	75.46	2.23	0.60	17.82	176.78
U1337	C	15	X	4	42	44	310.01	13.66	13.59	3.18	71.49	2.27	0.70	22.24	217.91
U1337	C	15	X	4	50	52	310.09	13.66	13.59	4.44	65.73	2.92	0.90	40.05	383.44
U1337	C	15	X	4	58	60	310.17	13.66	13.59	4.45	73.79	3.29	0.41	18.39	182.16
U1337	C	15	X	4	66	68	310.25	13.66	13.59	4.44	78.48	3.48	0.34	15.09	151.48
U1337	C	15	X	4	74	76	310.33	13.66	13.59	4.42	87.41	3.86	0.19	8.19	87.29
U1337	C	15	X	4	82	84	310.41	13.67	13.60	4.40	89.37	3.93	0.17	7.26	78.65
U1337	C	15	X	4	90	92	310.49	13.67	13.60	4.37	87.54	3.83	0.21	9.26	97.29
U1337	C	15	X	4	98	100	310.57	13.67	13.60	4.35	89.52	3.90	0.16	6.99	76.19
U1337	C	15	X	4	106	108	310.65	13.67	13.60	4.33	90.32	3.91	0.16	6.73	73.76
U1337	C	15	X	4	114	116	310.73	13.67	13.60	4.31	91.52	3.95	0.16	6.95	75.78
U1337	C	15	X	4	122	124	310.81	13.68	13.61	4.29	89.21	3.83	0.13	5.70	64.17
U1337	C	15	X	4	130	132	310.89	13.68	13.61	4.27	90.17	3.85	0.12	5.16	59.17
U1337	C	15	X	4	138	140	310.97	13.68	13.61	4.25	89.06	3.78	0.21	9.09	95.68
U1337	D	32	X	1	58	60	311.09	13.68	13.61	4.22	84.87	3.58	0.19	7.95	85.09
U1337	D	32	X	1	66	68	311.17	13.68	13.61	4.20	86.83	3.64	0.14	5.82	65.31
U1337	D	32	X	1	74	76	311.25	13.69	13.62	4.18	90.42	3.78	0.14	5.89	65.98
U1337	D	32	X	1	82	84	311.33	13.69	13.62	4.16	89.91	3.74	0.14	5.92	66.26
U1337	D	32	X	1	90	92	311.41	13.69	13.62	4.13	87.52	3.62	0.26	10.89	112.39

Site	Hole	Core	Type	Section	Top (cm)	Bottom (cm)	CCSF* (m)	Age** (Ma)	Shifted age (Ma)	MAR (g cm^{-2} kyr^{-1})	$CaCO_3$ weight %	CAR (g cm^{-2} kyr^{-1})	$BaSO_4$ weight %	BAR (mg cm^{-2} kyr^{-1})	Export C (gC m^{-2} yr^{-1})
U1337	D	32	X	1	98	100	311.49	13.69	13.62	4.11	87.34	3.59	0.22	9.23	96.97
U1337	D	32	X	1	106	108	311.57	13.69	13.62	4.09	90.49	3.70	0.16	6.52	71.81
U1337	D	32	X	1	114	116	311.65	13.69	13.62	4.07	91.92	3.74	0.13	5.18	59.35
U1337	D	32	X	1	122	124	311.73	13.70	13.63	4.08	89.07	3.63	0.24	9.60	100.44
U1337	D	32	X	1	130	132	311.81	13.70	13.63	4.09	81.54	3.33	0.52	21.07	207.00
U1337	D	32	X	1	138	140	311.89	13.70	13.63	4.09	78.33	3.21	0.60	24.47	238.64
U1337	D	32	X	2	2	4	312.03	13.70	13.63	4.10	84.75	3.48	0.27	11.16	114.95
U1337	D	32	X	2	6	8	312.07	13.70	13.63	4.10	86.76	3.56	0.21	8.54	90.61
U1337	D	32	X	2	14	16	312.15	13.71	13.64	3.51	83.46	2.93	0.30	10.66	110.31
U1337	D	32	X	2	22	24	312.23	13.71	13.64	3.46	80.33	2.78	0.49	17.07	169.85
U1337	D	32	X	2	30	32	312.31	13.71	13.64	3.47	83.64	2.90	0.18	6.20	68.82
U1337	D	32	X	2	38	40	312.39	13.71	13.64	3.47	90.90	3.16	0.11	3.89	47.32
U1337	D	32	X	2	46	48	312.47	13.71	13.64	3.48	89.97	3.13	0.07	2.26	32.23
U1337	D	32	X	2	54	56	312.55	13.72	13.65	3.48	88.46	3.08	0.08	2.92	38.37
U1337	D	32	X	2	62	64	312.63	13.72	13.65	3.49	87.85	3.06	0.16	5.61	63.34
U1337	D	32	X	2	70	72	312.71	13.72	13.65	3.49	88.84	3.10	0.18	6.46	71.23
U1337	D	32	X	2	78	80	312.79	13.72	13.65	3.50	87.21	3.05	0.18	6.20	68.85
U1337	D	32	X	2	86	88	312.87	13.72	13.65	3.50	88.77	3.11	0.18	6.22	69.05
U1337	D	32	X	2	102	104	313.03	13.73	13.66	3.51	90.34	3.17	0.14	4.83	56.05
U1337	D	32	X	2	110	112	313.11	13.73	13.66	3.52	87.70	3.08	0.21	7.50	80.94
U1337	D	32	X	2	118	120	313.19	13.73	13.66	3.52	88.03	3.10	0.17	5.98	66.74
U1337	D	32	X	2	126	128	313.27	13.73	13.66	3.53	92.00	3.24	0.12	4.35	51.60
U1337	D	32	X	2	134	136	313.35	13.74	13.67	3.52	91.22	3.21	0.14	5.10	58.62
U1337	D	32	X	2	142	144	313.43	13.74	13.67	3.52	86.77	3.05	0.24	8.49	90.12
U1337	D	32	X	3	2	4	313.53	13.74	13.67	3.51	85.06	2.99	0.16	5.60	63.27
U1337	D	32	X	3	6	8	313.57	13.74	13.67	3.51	90.29	3.17	0.15	5.34	60.81
U1337	D	32	X	3	14	16	313.65	13.74	13.67	3.48	87.47	3.04	0.12	4.05	48.88
U1337	D	32	X	3	30	32	313.81	13.75	13.68	3.01	78.30	2.36	0.56	16.76	167.01
U1337	D	32	X	3	38	40	313.89	13.75	13.68	3.01	75.57	2.27	0.61	18.29	181.21
U1337	D	32	X	3	54	56	314.05	13.76	13.69	3.00	80.27	2.41	0.42	12.51	127.48

Site	Hole	Core	Type	Section	Top (cm)	Bottom (cm)	CCSF* (m)	Age** (Ma)	Shifted age (Ma)	MAR (g cm^{-2} kyr^{-1})	$CaCO_3$ weight %	CAR (g cm^{-2} kyr^{-1})	$BaSO_4$ weight %	BAR (mg cm^{-2} kyr^{-1})	Export C (gC m^{-2} yr^{-1})
U1337	D	32	X	3	62	64	314.13	13.76	13.69	2.99	78.27	2.34	0.45	13.59	137.49
U1337	D	32	X	3	70	72	314.21	13.76	13.69	2.99	86.38	2.58	0.28	8.49	90.12
U1337	D	32	X	3	78	80	314.29	13.76	13.69	2.99	87.35	2.61	0.21	6.37	70.37
U1337	D	32	X	3	86	88	314.37	13.77	13.70	2.98	86.89	2.59	0.25	7.60	81.84
U1337	D	32	X	3	94	96	314.45	13.77	13.70	2.98	89.01	2.65	0.26	7.61	81.92
U1337	D	32	X	3	110	112	314.61	13.77	13.70	2.97	89.10	2.65	0.15	4.31	51.27
U1337	D	32	X	3	118	120	314.69	13.78	13.71	2.97	84.34	2.51	0.16	4.79	55.72
U1337	D	32	X	3	134	136	314.85	13.78	13.71	3.01	87.89	2.64	0.16	4.90	56.73
U1337	D	32	X	3	142	144	314.93	13.78	13.71	3.02	87.82	2.65	0.19	5.65	63.74
U1337	D	32	X	4	2	4	315.03	13.79	13.72	3.04	74.61	2.27	0.22	6.68	73.29
U1337	D	32	X	4	6	8	315.07	13.79	13.72	3.05	83.14	2.54	0.14	4.28	50.93
U1337	D	32	X	4	14	16	315.15	13.79	13.72	2.54	82.57	2.10	0.25	6.25	69.28
U1337	D	32	X	4	22	24	315.23	13.79	13.72	1.81	84.58	1.53	0.28	5.02	57.84
U1337	D	32	X	4	38	40	315.39	13.80	13.73	1.83	84.45	1.55	0.25	4.51	53.11
U1337	D	32	X	4	46	48	315.47	13.81	13.74	1.84	82.63	1.52	0.27	4.98	57.48
U1337	D	32	X	4	62	64	315.63	13.82	13.75	1.86	79.04	1.47	0.20	3.78	46.33
U1337	D	32	X	4	70	72	315.71	13.82	13.75	1.87	83.50	1.56	0.15	2.72	36.51
U1337	D	32	X	4	78	80	315.79	13.82	13.75	1.88	87.71	1.65	0.15	2.84	37.55
U1337	C	16	X	1	89	91	315.84	13.83	13.76	2.08	87.02	1.81	0.21	4.37	51.84
U1337	D	32	X	4	86	88	315.87	13.83	13.76	2.60	86.82	2.26	0.09	2.26	32.20
U1337	C	16	X	1	97	99	315.92	13.83	13.76	2.61	86.14	2.25	0.10	2.52	34.65
U1337	C	16	X	1	105	107	316.00	13.83	13.76	2.62	86.16	2.26	0.17	4.47	52.79
U1337	C	16	X	1	113	115	316.08	13.84	13.77	2.63	86.62	2.28	0.13	3.32	42.05
U1337	C	16	X	1	129	131	316.24	13.84	13.77	2.64	84.90	2.24	0.14	3.77	46.26
U1337	C	16	X	1	137	139	316.32	13.84	13.77	2.63	85.85	2.25	0.19	4.99	57.56
U1337	C	16	X	2	3	5	316.48	13.85	13.78	2.61	83.09	2.17	0.33	8.54	90.57
U1337	C	16	X	2	10	12	316.55	13.85	13.78	2.60	77.96	2.02	0.44	11.46	117.73
U1337	C	16	X	2	18	20	316.63	13.86	13.79	2.59	77.19	2.00	0.42	10.75	111.10
U1337	C	16	X	2	26	28	316.71	13.86	13.79	2.58	80.57	2.08	0.26	6.63	72.86
U1337	C	16	X	2	34	36	316.79	13.86	13.79	2.57	75.30	1.93	0.32	8.20	87.44

Site	Hole	Core	Type	Section	Top (cm)	Bottom (cm)	CCSF* (m)	Age** (Ma)	Shifted age (Ma)	MAR (g cm^{-2} kyr^{-1})	$CaCO_3$ weight %	CAR (g cm^{-2} kyr^{-1})	$BaSO_4$ weight %	BAR (mg cm^{-2} kyr^{-1})	Export C (gC m^{-2} yr^{-1})
U1337	C	16	X	2	42	44	316.87	13.86	13.79	2.56	77.66	1.99	0.21	5.49	62.21
U1337	C	16	X	2	50	52	316.95	13.87	13.80	2.20	79.55	1.75	0.42	9.22	96.91
U1337	C	16	X	2	58	60	317.03	13.87	13.80	2.19	84.19	1.85	0.38	8.37	88.95
U1337	C	16	X	2	66	68	317.11	13.87	13.80	2.18	85.54	1.87	0.23	4.99	57.59
U1337	C	16	X	2	74	76	317.19	13.88	13.81	2.18	86.74	1.89	0.11	2.46	34.06
U1337	C	16	X	2	82	84	317.27	13.88	13.81	2.17	66.52	1.44	0.26	5.58	63.08
U1337	C	16	X	2	90	92	317.35	13.89	13.82	2.16	47.85	1.03	0.44	9.45	99.02
U1337	C	16	X	2	98	100	317.43	13.89	13.82	2.15	63.67	1.37	0.26	5.67	63.85
U1337	C	16	X	2	122	124	317.67	13.90	13.83	2.12	30.49	0.65	1.91	40.50	387.62
U1337	C	16	X	2	130	132	317.75	13.90	13.83	2.13	57.48	1.22	0.72	15.32	153.62
U1337	C	16	X	2	138	140	317.83	13.91	13.84	2.10	31.19	0.65	0.36	7.50	80.93
U1337	C	16	X	2	146	148	317.91	13.91	13.84	1.53	60.44	0.92	0.54	8.31	88.40
U1337	C	16	X	3	2	4	317.97	13.91	13.84	1.53	75.71	1.16	0.45	6.92	75.50
U1337	C	16	X	3	10	12	318.05	13.92	13.85	1.53	85.56	1.31	0.30	4.60	53.96
U1337	C	16	X	3	18	20	318.13	13.92	13.85	1.53	85.79	1.32	0.18	2.73	36.59
U1337	C	16	X	3	26	28	318.21	13.93	13.86	1.54	85.41	1.31	0.12	1.79	27.84
U1337	C	16	X	3	34	36	318.29	13.93	13.86	1.54	80.26	1.23	0.22	3.44	43.21
U1337	C	16	X	3	42	44	318.37	13.94	13.87	1.54	88.95	1.37	0.12	1.85	28.43
U1337	C	16	X	3	50	52	318.45	13.94	13.87	1.54	88.84	1.37	0.12	1.80	27.97
U1337	C	16	X	3	58	60	318.53	13.95	13.88	1.20	90.37	1.08	0.13	1.53	25.43
U1337	C	16	X	3	66	68	318.61	13.95	13.88	1.14	89.85	1.02	0.13	1.49	25.08
U1337	C	16	X	3	74	76	318.69	13.96	13.89	1.14	90.12	1.03	0.15	1.74	27.34
U1337	C	16	X	3	82	84	318.77	13.97	13.90	1.14	88.80	1.01	0.14	1.56	25.70
U1337	C	16	X	3	90	92	318.85	13.97	13.90	1.14	88.69	1.01	0.11	1.29	23.23
U1337	C	16	X	3	98	100	318.93	13.98	13.91	1.14	87.15	1.00	0.16	1.89	28.72
U1337	C	16	X	3	106	108	319.01	13.99	13.92	1.18	26.96	0.32	0.30	3.54	44.07
U1337	C	16	X	3	114	116	319.09	13.99	13.92	1.75	82.39	1.44	0.39	6.88	75.13
U1337	C	16	X	3	122	124	319.17	14.00	13.93	1.75	79.19	1.39	0.50	8.69	91.94
U1337	C	16	X	3	138	140	319.33	14.01	13.94	1.75	78.42	1.38	0.49	8.66	91.69
U1337	C	16	X	3	146	148	319.41	14.01	13.94	1.76	82.65	1.45	0.31	5.45	61.88

Site	Hole	Core	Type	Section	Top (cm)	Bottom (cm)	CCSF* (m)	Age** (Ma)	Shifted age (Ma)	MAR (g cm^{-2} kyr^{-1})	$CaCO_3$ weight %	CAR (g cm^{-2} kyr^{-1})	$BaSO_4$ weight %	BAR (mg cm^{-2} kyr^{-1})	Export C (gC m^{-2} yr^{-1})
U1337	C	16	X	4	2	4	319.47	14.01	13.94	1.76	76.75	1.35	0.43	7.61	81.93
U1337	C	16	X	4	10	12	319.55	14.02	13.95	1.76	69.73	1.23	0.39	6.90	75.31
U1337	C	16	X	4	18	20	319.63	14.02	13.95	1.76	56.76	1.00	0.31	5.44	61.79
U1337	A	32	X	1	102	102	319.66	14.02	13.95	1.78	61.98	1.10	0.61	10.84	111.98
U1337	A	32	X	1	108	110	319.72	14.03	13.96	1.78	67.70	1.20	0.52	9.16	96.36
U1337	A	32	X	1	118	120	319.82	14.03	13.96	2.57	51.04	1.31	0.66	16.88	168.06
U1337	A	32	X	1	128	130	319.92	14.03	13.96	2.57	7.86	0.20	0.56	14.30	144.08
U1337	A	32	X	2	2	4	320.16	14.04	13.97	2.58	37.90	0.98	0.77	19.97	196.85
U1337	A	32	X	2	12	14	320.26	14.05	13.98	2.58	46.28	1.20	0.70	17.98	178.28
U1337	A	32	X	2	22	24	320.36	14.05	13.98	2.59	34.19	0.89	0.50	12.96	131.65
U1337	A	32	X	2	32	34	320.46	14.05	13.98	2.59	38.27	0.99	0.87	22.49	220.27
U1337	A	32	X	2	42	44	320.56	14.06	13.99	2.60	36.71	0.95	0.82	21.32	209.40
U1337	A	32	X	2	52	54	320.66	14.06	13.99	2.60	63.40	1.65	0.41	10.61	109.82
U1337	A	32	X	2	68	70	320.82	14.07	14.00	2.61	81.42	2.12	0.11	2.88	37.96
U1337	A	32	X	2	82	84	320.96	14.08	14.01	1.61	83.20	1.34	0.14	2.26	32.16
U1337	A	32	X	2	92	94	321.06	14.08	14.01	1.60	84.77	1.36	0.12	1.91	28.92
U1337	A	32	X	2	108	110	321.22	14.09	14.02	1.53	74.57	1.14	0.28	4.31	51.26

*From Wilkens et al. (2012)
**From Tian et al. (2013)